Fluid Antenna-Aided Rate-Splitting Multiple Access

Farshad Rostami Ghadi, *Member*, *IEEE*, Kai-Kit Wong, *Fellow*, *IEEE*,
F. Javier López-Martínez, *Senior Member*, *IEEE*, Lajos Hanzo, *Life Fellow*, *IEEE*, and
Chan-Byoung Chae, *Fellow*, *IEEE*

***Abstract*—This letter considers a fluid antenna system (FAS)-aided rate-splitting multiple access (RSMA) approach for downlink transmission. In particular, a base station (BS) equipped with a single traditional antenna system (TAS) uses RSMA signaling to send information to several mobile users (MUs) each equipped with FAS. To understand the achievable performance, we first present the distribution of the equivalent channel gain based on the joint multivariate t-distribution and then derive a compact analytical expression for the outage probability (OP). Moreover, we obtain the asymptotic OP in the high signal-to-noise ratio (SNR) regime. Numerical results show that combining FAS with RSMA significantly outperforms TAS and conventional multiple access schemes, such as non-orthogonal multiple access (NOMA), in terms of OP. The results also indicate that FAS can be the tool that greatly improves the practicality of RSMA.**

***Index Terms*—Downlink, fluid antenna system (FAS), outage probability, rate-splitting multiple access (RSMA).**

I. Introduction

THE RAPID advance of wireless communication systems is driven by the growing demand for sophisticated multimedia applications. Hence, next-generation networks (NGNs), a.k.a. the sixth-generation (6G), are aimed to support increased spectral efficiency, massive connectivity, and enhanced quality of service (QoS), including ultra-reliable low-latency communications (URLLC) and real-time data processing [1]. Among the innovative solutions being explored, such as ultra-massive multiple-input multiple-output (UM-MIMO) systems, reconfigurable intelligent surfaces (RIS), and integrated sensing and communications (ISAC), fluid antenna system (FAS) appears to be the latest breakthrough driven by new reconfigurability in antenna such as shape and position [2], [3].

The work of F. Rostami Ghadi and K. K. Wong is supported by the Engineering and Physical Sciences Research Council (EPSRC) under Grant EP/W026813/1. The work of F. J. López-Martínez is funded in part by Junta de Andalucía through grant EMERGIA20-00297, and in part by MICIU/AEI/10.13039/50110001103 and FEDER/UE through grant PID2023-149975OB-I00 (COSTUME). L. Hanzo would like to acknowledge the financial support of the EPSRC projects under grant EP/Y026721/1, EP/W032635/1, EP/Y037243/1 and EP/X04047X/1 as well as of the European Research Council's Advanced Fellow Grant QuantCom (Grant No. 789028). The work of C.-B. Chae is supported by the Institute for Information and Communication Technology Planning and Evaluation (IITP)/NRF grant funded by the Ministry of Science and ICT (MSIT), South Korea, under Grant RS-2024-00428780 and 2022R1A5A1027646.

F. Rostami Ghadi and K. K. Wong are with the Department of Electronic and Electrical Engineering, University College London, London, UK. (e-mail: {f.rostamighadi, kai-kit.wong}@ucl.ac.uk). K. K. Wong is also affiliated with Yonsei Frontier Lab, Yonsei University, Seoul, Korea.

F. J. López-Martínez is with the Department of Signal Theory, Networking and Communications, Research Centre for Information and Communication Technologies (CITIC-UGR), University of Granada, 18071, Granada (Spain). (e-mail: fjlm@ugr.es).

L. Hanzo is with the School of Electronics and Computer Science, University of Southampton, Southampton, U.K. (e-mail: lh@ecs.soton.ac.uk).

C. B. Chae is with Yonsei Frontier Lab, Yonsei University, Seoul, Korea. (e-mail: cbchae@yonsei.ac.kr).

Corresponding author: Kai-Kit Wong.

In contrast to traditional antenna system (TAS), FAS offers a new degree-of-freedom to the physical layer, and therefore can significantly enhance both the diversity and multiplexing gains [4], [5]. By leveraging the unique capabilities of FAS, substantial efforts have recently been devoted to integrating it with cutting-edge technologies, such as MIMO [5], [6], RIS [7], and ISAC [8], among others. Experimental results on FAS have also been reported recently in [9].

A key application that FAS may find being very useful is the multiuser communication scenarios where spectrally efficient techniques such as non-orthogonal multiple access (NOMA) and rate-splitting multiple access (RSMA) are utilized. NOMA allows multiple mobile users (MUs) to share the same physical channel to boost its overall spectral efficiency but relies on the use of successive interference cancellation (SIC) at the MUs. Similar to NOMA, RSMA has been piped to do the same or better with a more general and robust transmission framework [10]. RSMA splits MUs' data into common and private message components that are transmitted simultaneously, allowing for more effective interference mitigation [11]. But regardless, interference cancellation is an important part for both NOMA and RSMA, where FAS could shine due to its massive spatial diversity. Note that in [12], FAS has been shown to bring down the power consumption a lot when combined with NOMA.

In this letter, we investigate the integration of FAS with the RSMA scheme, focusing on how this combination can enhance communication reliability and performance in scenarios with multiple MUs and varying channel conditions. Specifically, we examine a multiuser downlink wireless communication system in which MUs employ FAS, while the base station (BS) is equipped with a TAS to adopt the RSMA scheme to simultaneously serve these MUs. We first derive the distribution of the equivalent received channel gain at the FAS-equipped MUs and then characterize the outage probability (OP) in terms of the joint cumulative distribution function (CDF) of the multivariate t-distribution using a copula-based formulation. Fig. 1 illustrates a flowchart outlining the key mathematical derivations in this letter. Hence, the main novelties and contributions of our work are summarized as follows:

- **First study on RSMA in the context of FAS:** To the best of our knowledge, this work is the first to analyze RSMA with FAS, introducing a novel integration that enables adaptive antenna positioning for enhanced spectral efficiency and user fairness. In contrast to conventional RSMA approaches that rely on fixed-position antenna systems, our study exploits the flexibility of FAS to dynamically adjust the antenna locations based on real-time channel conditions.
- **Novel channel correlation modeling using a joint multivariate t-distribution:** We develop a new correlation model that better captures the dependencies and tail

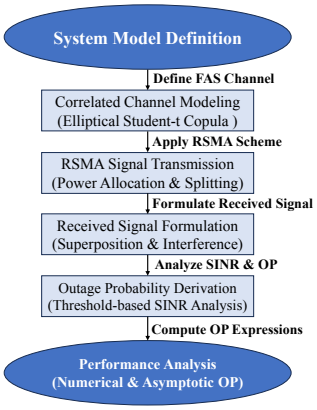

Fig. 1. Flowchart of the key mathematical steps.

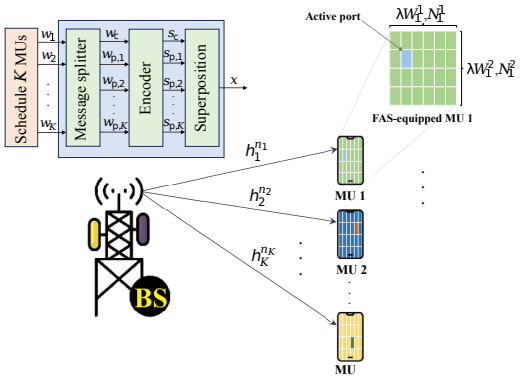

Fig. 2. A sketch of the FAS-aided RSMA model.

behavior of small-scale fading, unlike existing Gaussian-based models. This provides a more generalized and accurate representation of practical wireless environments under correlated fading.

- **Comprehensive benchmarking and performance evaluation:** Unlike previous studies that focus solely on FAS-NOMA or TAS-based schemes, we systematically compare FAS-RSMA with multiple benchmark schemes, e.g., TAS-RSMA, FAS-NOMA, and TAS-NOMA, to quantify its advantages over both traditional NOMA and RSMA architectures. Our analysis reveals that the integration of FAS with RSMA outperforms the configurations where MUs utilize TAS, and offers additional flexibility and robustness compared to the case where the BS employs NOMA signalling. This highlights the advantages of combining fluid antenna technology with innovative multiple access methods to enhance overall efficiency.

II. System Model

A. Channel Model

Consider the downlink of a FAS-aided RSMA communication setup as shown in Fig. 2, which consists of a TAS-equipped BS and K FAS-equipped MUs u_k[1], for $k = 1,\ldots,K$. Each MU u_k features a grid structure consisting of N_k^l ports, uniformly distributed over two linear spaces of length $W_k^l\lambda$ for $l \in \{1,2\}$, with λ being the carrier wavelength. As a result, the total number of ports for MU u_k is $N_k = N_k^1 \times N_k^2$ and the total area of the surface is $W_k = \left(W_k^1 \times W_k^2\right)\lambda^2$. To simplify our notations, we introduce a mapping function $\mathcal{F}\left(n_k\right) = \left(n_k^1, n_k^2\right)$, also $n_k = \mathcal{F}^{-1}\left(n_k^1, n_k^2\right)$, which converts the two-dimensional (2D) indices into a one-dimensional (1D) form such that $n_k \in \{1,\ldots,N_k\}$ and $n_k^l \in \left\{1,\ldots,N_k^l\right\}$. The complex channels from the BS to MU u_k can be modeled as [12]

$$\mathbf{h}_k = \sqrt{\frac{\mathfrak{K}}{\mathfrak{K}+1}}\mathrm{e}^{j\omega}\mathbf{a}\left(\theta_{0,k},\psi_{0,k}\right) + \sqrt{\frac{1}{\left(\mathfrak{K}+1\right)}}\sum_{\mathfrak{l}=1}^{\mathfrak{L}}\kappa_{\mathfrak{l},k}\mathbf{a}\left(\theta_{\mathfrak{l},k},\psi_{\mathfrak{l},k}\right), \quad (1)$$

[1]In this work, we assume that FAS is implemented at the MUs rather than the BS. This choice is motivated by two key reasons: operational simplicity, and consistence with state-of-the art approaches used for benchmarking.

where $\mathfrak{K}$ represents the Rice factor, ω denotes the phase of the line-of-sight (LoS) component, $\mathfrak{L}$ denotes the number of scattered paths, $\kappa_{\mathfrak{l},k}$ indicates the complex channel coefficient of the $\mathfrak{l}$-th scattered component, and $\mathbf{a}$ is the receive steering vector, which is defined as

$$\begin{aligned}&\mathbf{a}\left(\theta_{\mathfrak{l},k},\psi_{\mathfrak{l},k}\right)\\ &= \begin{bmatrix}1 & \mathrm{e}^{j\frac{2\pi W_k^1}{N_k^1-1}\sin\theta_{\mathfrak{l},k}\cos\psi_{\mathfrak{l},k}} & \ldots & \mathrm{e}^{j2\pi W_k^1\sin\theta_{\mathfrak{l},k}\cos\psi_{\mathfrak{l},k}}\end{bmatrix}^T\\ &\otimes\begin{bmatrix}1 & \mathrm{e}^{j\frac{2\pi W_k^2}{N_k^2-1}\sin\theta_{\mathfrak{l},k}\cos\psi_{\mathfrak{l},k}} & \ldots & \mathrm{e}^{j2\pi W_k^2\sin\theta_{\mathfrak{l},k}\cos\psi_{\mathfrak{l},k}}\end{bmatrix}, \quad (2)\end{aligned}$$

where $\theta_{\mathfrak{l},k}$ and $\psi_{\mathfrak{l},k}$ denote the azimuth and elevation angle-of-arrival, respectively, and $\otimes$ is the Kronecker tensor product. It is worth mentioning that by assuming $\mathfrak{L}\to\infty$ and $\mathfrak{K}=0$, the magnitude of each entry of $\mathbf{h}_k$ follows Rayleigh fading. Therefore, given that the fluid antenna ports can freely switch to any position and be arbitrarily close to each other, the corresponding channels are spatially correlated. More specifically, the covariance between two arbitrary ports $n_k = \mathcal{F}^{-1}\left(n_k^1, n_k^2\right)$ and $\tilde{n}_k = \mathcal{F}^{-1}\left(\tilde{n}_k^1, \tilde{n}_k^2\right)$ at MU u_k for the considered scenario under rich scattering is given by [5]

$$\varrho_{n_k,\tilde{n}_k} = \mathcal{J}_0\left(2\pi\sqrt{\left(\frac{n_k^1-\tilde{n}_k^1}{N_k^1-1}W_k^1\right)^2+\left(\frac{n_k^2-\tilde{n}_k^2}{N_k^2-1}W_k^2\right)^2}\right), \quad (3)$$

where $\mathcal{J}_0\left(\cdot\right)$ defines the zero-order spherical Bessel function of the first kind.

B. Signal Model

As illustrated in Fig. 2, it is assumed that the BS exploits RSMA signalling for simultaneously supporting K MUs such that messages w_k are transmitted to MUs u_k. Given the RSMA principle, w_k is split into the common message w_c and private message $w_{\mathrm{p},k}$. A shared codebook between MUs is used to jointly encode w_c into a common stream s_c, which must be decoded by all MUs. Simultaneously, $w_{\mathrm{p},k}$ are encoded into the respective private streams s_p. Consequently, the signal transmitted by the BS to the n-th port of each MU is

$$x^{n_k} = \sqrt{P}\left(\sqrt{\alpha_\mathrm{c}}s_\mathrm{c} + \sum_{k=1}^{K}\sqrt{\alpha_{\mathrm{p},k}}s_{\mathrm{p},k}\right), \quad (4)$$

where P denotes the transmit power, while $\alpha_{\rm c}$ and $\alpha_{{\rm p},k}$ represent the power allocation factors for $s_{\rm c}$ and $s_{{\rm p},k}$, respectively, so that $\alpha_{\rm c}+\sum_{k=1}^{K}\alpha_{{\rm p},k}=1$. Therefore, the received signal at the n-th port of the k-th MU can be expressed as

$$\begin{aligned} y_k^{n_k} &= h_k^{n_k}x^{n_k}+z_k^{n_k} \\ &= \underbrace{\sqrt{PL_k\alpha_{\rm c}}h_k^{n_k}s_{\rm c}}_{\text{common message}}+\underbrace{\sqrt{PL_k\alpha_{{\rm p},k}}h_k^{n_k}s_{{\rm p},k}}_{\text{private message}} \\ &\quad+\underbrace{\sum_{\substack{\tilde{k}=1\\ \tilde{k}\neq k}}^{K}\sqrt{PL_k\alpha_{{\rm p},\tilde{k}}}h_k^{n_k}s_{{\rm p},\tilde{k}}}_{\text{interference}}+z_k^{n_k}, \end{aligned} \tag{5}$$

in which $h_k^{n_k}$ is the fading channel coefficient at the n-th port of MU ${\rm u}_k$, $z_k^{n_k}$ denotes the complex additive white Gaussian noise (AWGN) with zero mean and variance of σ^2, and $L_k=d_k^{-\beta}$ represents the path-loss, where $\beta>2$ is the path-loss exponent and d_k denotes the Euclidean distance between the BS placed at (X_0,Y_0,Z_0) and the k-th MU located at (X_k,Y_k,Z_k), which can be determined as

$$d_k=\sqrt{(X_0-X_k)^2+(Y_0-Y_k)^2+(Z_0-Z_k)^2}. \tag{6}$$

C. Signal-to-Interference Plus Noise Ratio (SINR)

It is evident from (5) that in addition to the common and intended private messages, each MU also receives the private messages intended for other MUs. This contributes to the interference level, complicating the decoding of the desired messages. To mitigate this, each MU employs a two-step decoding process for extracting the intended information from the received signal. In the initial step, the MU focuses on decoding the common message, while treating all private messages as noise. Following the FAS concept, we assume that only the optimal port that maximizes the received SINR at the FAS-equipped MUs is activated.[2] Therefore, the SINR for the k-th MU can be mathematically expressed as

$$\gamma_{{\rm c},k}=\frac{\overline{\gamma}\alpha_{\rm c}L_k\left|h_k^{n_k^*}\right|^2}{\overline{\gamma}\left(1-\alpha_{\rm c}\right)L_k\left|h_k^{n_k^*}\right|^2+1}, \tag{7}$$

in which $\overline{\gamma}=\frac{P}{\sigma^2}$ defines the average transmit signal-to-noise ratio (SNR) and n_k^* denotes the best port index at MU ${\rm u}_k$ that maximizes the channel gain, i.e.,

$$n_k^*=\arg\max_{n}\left\{|h_k^{n_k}|^2\right\}. \tag{8}$$

Thus, the equivalent channel gain at MU ${\rm u}_k$ is given by

$$g_{{\rm fas},k}=\max\left\{g_k^1,\ldots,g_k^{N_k}\right\}, \tag{9}$$

where $g_k^{n_k}=|h_k^{n_k}|^2$.

[2]The analysis assumes a conventional port selection scheme based on the highest received signal strength, which can be implemented using state-of-the-art channel estimation and reconstruction techniques based on linear filtering [13]. Alternative port selection schemes may require more sophisticated optimization algorithms with the possibility of better performance, establishing a trade-off between complexity and performance improvement [14].

In the second stage of the RSMA scheme, after successfully decoding the common message, each MU moves on to decode its own private message. This is achieved by subtracting the decoded common message from the received signal, while treating the private messages intended for other MUs as noise[3]. At this point, the MU focuses on isolating its desired private message. Hence, the SINR for decoding the private message at the k-th FAS-equipped MU can then be expressed as

$$\gamma_{{\rm p},k}=\frac{\overline{\gamma}\alpha_{{\rm p},k}L_k\left|h_k^{n_k^*}\right|^2}{\overline{\gamma}L_k\left|h_k^{n_k^*}\right|^2\sum_{\substack{\tilde{k}=1\\ \tilde{k}\neq k}}^{K}\alpha_{{\rm p},k}+1}. \tag{10}$$

III. Performance Analysis

Here, we first derive the CDF and the probability density function (PDF) of the received SINR at the MUs, for the case of Rayleigh fading. We then provide the OP expression, along with its asymptotic form in the high-SNR regime.

A. SINR Distribution

Given (9), the CDF of the channel gain at the FAS-RSMA MU ${\rm u}_k$ can be mathematically defined as

$$\begin{aligned} F_{g_{{\rm fas},k}}(g) &= \Pr\left(\max\left\{g_k^1,\ldots,g_k^{N_k}\right\}\leq g\right) && (11)\\ &= \Pr\left(g_k^1\leq g,\ldots,g_k^{N_k}\leq g\right) && (12)\\ &= F_{g_k^1,\ldots,g_k^{N_k}}(g,\ldots,g), && (13) \end{aligned}$$

where (13) is the joint multivariate CDF of N_k correlated exponential random variables (RVs) due to the spatial correlation between the corresponding Rayleigh channel coefficients. It is evident that deriving the closed-from expression of $F_{g_{{\rm fas},k}}(g)$ is mathematically intractable. Nevertheless, the joint CDF of arbitrary multivariate RVs can be efficiently generated by using Sklar's theorem such that for d arbitrary correlated RVs S_i, $i=1,\ldots,d$, associated with the univariate marginal CDF $F_{S_i}(s_i)$, the joint multivariate CDF $F_{S_1,\ldots,S_d}(s_1,\ldots,s_d)$, in the extended real line domain $\overline{\mathbb{R}}$, is given by [15]

$$F_{S_1,\ldots,S_d}(s_1,\ldots,s_d)=C\left(F_{S_1}(s_1),\ldots,F_{S_d}(s_d);\Theta\right). \tag{14}$$

In (14), $C(\cdot):[0,1]^d\rightarrow[0,1]$ denotes the copula function that is a joint CDF of d random vectors on the unit cube $[0,1]^d$ associated with uniform marginal distributions, i.e.,

$$C(u_1,\ldots,u_d;\Theta)=\Pr\left(U_1\leq u_1,\ldots,U_d\leq u_d\right). \tag{15}$$

in which $u_i=F_{S_i}(s_i)$ and Θ denotes the dependence parameter, which characterizes the dependency between the respective correlated RVs. Following [15], it was revealed in [16] that the elliptical copula accurately captures the spatial correlation in FAS, where the corresponding CDF can be expressed in terms

[3]For the sake of a fair comparison with other benchmarking schemes, ideal signal processing capabilities like perfect decoding and perfect channel knowledge are assumed, while interference and additive noise are explicitly considered in the received signal model. Although ideal assumptions are useful to establish performance bounds, it is acknowledged that practical implementations would encounter imperfections such as channel estimation errors and interference management challenges that require further consideration.

of the Gaussian copula, i.e., the joint multivariate CDF of normal distribution. Although the Gaussian copula is capable of accurately describing the structure of dependency between the fading coefficients, it cannot cover heavy tail dependencies, where deep fading occurs. To overcome this issue, we utilize a more general elliptical student-t copula, which includes an additional parameter ν_k in addition to the correlation matrix, to control the degree of tail dependencies.

Proposition 1. *The CDF and PDF of the equivalent channel gain $g_{\mathrm{fas},k}$ at MU u_k for FAS-RSMA are given by*

$$F_{g_{\mathrm{fas},k}}(g) = T_{\nu_k,\mathbf{\Sigma}_k}\left(t_{\nu_k}^{-1}\left(1-\mathrm{e}^{-\frac{g}{\overline{g}}}\right),\ldots,t_{\nu_k}^{-1}\left(1-\mathrm{e}^{-\frac{g}{\overline{g}}}\right);\nu_k,\Theta_k\right), \tag{16}$$

$$f_{g_{\mathrm{fas},k}}(g) = \frac{1}{\overline{g}}\exp\left(-\frac{g}{\overline{g}}\right) \times\left[\sum_{n_k=1}^{N_k} T_{\nu_k+1,\,\widetilde{\mathbf{\Sigma}}_{k,n_k}}\left(\frac{t_{\nu_k}^{-1}\left(1-\mathrm{e}^{-\frac{g}{\overline{g}}}\right)\left(\mathbf{1}_{N_k-1}-\boldsymbol{\rho}_{k,n_k}\right)}{\sqrt{\frac{\nu_k+\left[t_{\nu_k}^{-1}\left(1-\mathrm{e}^{-g/\overline{g}}\right)\right]^2}{\nu_k+1}}}\right)\right], \tag{17}$$

where $\overline{g}=\mathbb{E}[g]$ is the mean of the channel gain, $t_{\nu_k}^{-1}(\cdot)$ is the inverse CDF (quantile function) of the univariate t-distribution having ν_k degrees of freedom for the k-th MU, $T_{\nu_k,\mathbf{\Sigma}_k}(\cdot)$ represents the CDF of the multivariate t-distribution with correlation matrix $\mathbf{\Sigma}_k$ and ν_k degrees of freedom for the k-th MU, and $\Theta_k\in[-1,1]$ denotes the dependence parameter of the t-student copula, which represents the correlation between the n_k-th and $\tilde{n}_k$-th ports in $\mathbf{\Sigma}_k$. Moreover, $T_{\nu_k+1,\,\widetilde{\mathbf{\Sigma}}_{k,n_k}}$ is the (N_k-1)-variate t CDF, $\boldsymbol{\rho}_{k,n_k}$ denotes the n_k-th column of $\mathbf{\Sigma}_k$ without its n_k-th entry, and the term $\widetilde{\mathbf{\Sigma}}_{k,n_k}=\mathbf{D}_{k,n_k}^{-1/2}\mathbf{S}_{k,n_k}\mathbf{D}_{k,n_k}^{-1/2}$ is the conditional correlation matrix of the (N_k-1) remaining coordinates given the n_k-th one with $\mathbf{S}_{k,n_k}=\mathbf{\Sigma}_{k,-n_k,-n_k}-\boldsymbol{\rho}_{k,n_k}\boldsymbol{\rho}_{k,n_k}^{\top}$ and $\mathbf{D}_{k,n_k}=\mathrm{diag}(\mathbf{S}_{k,n_k})$. Besides, $\mathbf{1}_{N_k-1}=(1,\ldots,1)^{\top}\in\mathbb{R}^{N_k-1}$ in which $\mathbb{R}^{N_k-1}$ is the set of all column vectors of length N_k-1 whose entries are real numbers.

Proof. See Appendix A. □

Remark 1. *The choice of the multivariate t-distribution for modeling the equivalent channel gain is motivated by its ability to capture heavy-tailed fading characteristics, which are common in practical wireless environments. Unlike the Gaussian model, the t-distribution provides increased flexibility by accounting for non-Gaussian fading conditions while maintaining analytical tractability. Moreover, its ability to model spatially correlated signals makes it particularly suitable for FAS-based communication systems. While alternative models such as non-parametric distributions could be explored, they often lack closed-form solutions, making analytical performance evaluation intractable. Our framework, however, remains extendable to accommodate more general fading distributions if desired.*

B. OP Analysis

The OP is a key performance metric in wireless communications, defined as the probability that the received SNR or SINR falls below a critical threshold, causing a disruption of reliable communication. In the RSMA-based signaling model, since each MU receives a combination of a common message and its own private message, along with the private messages intended for other MUs, and decodes both messages through a two-step decoding process, an outage occurs when the SINRs of decoding either the common or private message drop below their respective thresholds denoted as $\gamma_{\mathrm{th,c}}$ for the common message and $\gamma_{\mathrm{th,p}}$ for the private message.

Proposition 2. *The OP of MU k in FAS-RSMA is given by*

$$P_{\mathrm{o},k} = T_{\nu_k,\mathbf{\Sigma}_k}\left(t_{\nu_k}^{-1}\left(1-e^{-\frac{\gamma_{\mathrm{th}}^k}{\overline{g}}}\right),\ldots,t_{\nu_k}^{-1}\left(1-e^{-\frac{\gamma_{\mathrm{th}}^k}{\overline{g}}}\right);\nu_k,\Theta_k\right), \tag{18}$$

where $\gamma_{\mathrm{th}}^k=\max\left\{\hat{\gamma}_{\mathrm{th,c}}^k,\hat{\gamma}_{\mathrm{th,p}}^k\right\}$ in which $\hat{\gamma}_{\mathrm{th,c}}^k=\frac{\gamma_{\mathrm{th,c}}^k}{\overline{\gamma}L_k\left(\alpha_{\mathrm{c}}-(1-\alpha_{\mathrm{c}})\gamma_{\mathrm{th,c}}^k\right)}$ and $\hat{\gamma}_{\mathrm{th,p}}^k=\frac{\gamma_{\mathrm{th,p}}^k}{\overline{\gamma}L_k\left(\alpha_{\mathrm{p},k}-(1-\alpha_{\mathrm{c}}-\alpha_{\mathrm{p},k})\gamma_{\mathrm{th,p}}^k\right)}$.

Proof. Given the definition, the OP at the k-th FAS-equipped RSMA MU can be expressed mathematically as

$$\begin{aligned}
P_{\mathrm{o},k} &= 1-\Pr\left(\gamma_{\mathrm{c},k}>\gamma_{\mathrm{th,c}}^k,\gamma_{\mathrm{p},k}>\gamma_{\mathrm{th,p}}^k\right) && \text{(19a)}\\
&= 1-\Pr\left(\frac{\overline{\gamma}\alpha_{\mathrm{c}}L_k g_{\mathrm{fas},k}}{\overline{\gamma}\left(1-\alpha_{\mathrm{c}}\right)L_k g_{\mathrm{fas},k}+1}>\gamma_{\mathrm{th,c}}^k,\right.\\
&\qquad \left.\frac{\overline{\gamma}\alpha_{\mathrm{p},k}L_k g_{\mathrm{fas},k}}{\overline{\gamma}L_k g_{\mathrm{fas},k}\sum_{\tilde{k}=1,\tilde{k}\neq k}^{K}\alpha_{\mathrm{p},k}+1}>\gamma_{\mathrm{th,p}}^k\right) && \text{(19b)}\\
&= 1-\Pr\left(g_{\mathrm{fas},k}>\hat{\gamma}_{\mathrm{th,c}}^k,g_{\mathrm{fas},k}>\hat{\gamma}_{\mathrm{th,p}}^k\right) && \text{(19c)}\\
&= \Pr\left(g_{\mathrm{fas},k}\leq\max\left\{\hat{\gamma}_{\mathrm{th,c}}^k,\hat{\gamma}_{\mathrm{th,p}}^k\right\}\right) && \text{(19d)}\\
&= F_{g_{\mathrm{fas},k}}\left(\gamma_{\mathrm{th}}^k\right), && \text{(19e)}
\end{aligned}$$

where (19b) is derived by substituting (7) and (10) into (19a), while (19e) is derived by using (16). □

Corollary 1. *The asymptotic OP in the high-SNR regime for the considered FAS-RSMA is given by*

$$P_{\mathrm{o},k}^{\infty} = T_{\nu_k,\mathbf{\Sigma}_k}\left(t_{\nu_k}^{-1}\left(\frac{\gamma_{\mathrm{th}}}{\overline{g}}\right),\ldots,t_{\nu_k}^{-1}\left(\frac{\gamma_{\mathrm{th}}}{\overline{g}}\right);\nu_k,\Theta_k\right). \tag{20}$$

Proof. Given that the channel gains are distributed exponentially, we can derive their respective CDFs at high SNR by employing the Taylor series expansion. Hence, when $\overline{\gamma}\to\infty$, the term $\mathrm{e}^{\gamma_{\mathrm{th}}/\overline{g}}$ becomes very small, so we have $F_{g_k^{n_k}}^{\infty}(\gamma_{\mathrm{th}})\approx\gamma_{\mathrm{th}}/\overline{g}$. Consequently, by inserting the obtained marginal CDF $F_{g_k^{n_k}}^{\infty}(\gamma_{\mathrm{th}})$ into (18), the proof is completed. □

Remark 2. *The combination of FAS and RSMA offers distinct advantages over standalone FAS systems. Similarly to the case of FAS-NOMA [12], in FAS-RSMA, the BS can decode both a common message and private messages through SIC, improving interference management and spectral efficiency with respect to standalone FAS.*

IV. Numerical Results

Here, we evaluate the OP performance of FAS-RSMA. Unless otherwise specified, we set the system parameters to $\beta = 2.1$, $\alpha_{\rm c} = 0.7$, $W_k = 1\lambda^2$, $N_k = 4$, $\nu = 40$, and $\gamma^k_{\rm th,c} = \gamma^k_{\rm th,p} = 0$ dB. For the sake of simplicity in the simulations, we consider a two-user FAS-RSMA, i.e., $K = 2$[4], where the BS is placed at the origin $(0, 0, 0)$, and MUs u_1 and u_2 are positioned at $(50, 50, 0)$m and $(10, 50, 0)$m, respectively. The corresponding power allocation factors for the private messages are $\alpha_{\rm p,1} = 0.75\,(1 - \alpha_{\rm c})$ and $\alpha_{\rm p,2} = 0.25\,(1 - \alpha_{\rm c})$. Furthermore, we use the MATLAB function `copulacdf` to implement the t-student copula, which is expressed in terms of the joint CDF of the multivariate t-distribution. We also consider the following schemes as the benchmark:

- **FAS-NOMA:** MUs employ a FAS-aided NOMA.
- **TAS-RSMA:** MUs rely on a TAS-aided RSMA.
- **TAS-NOMA:** MUs adopt a TAS-aided NOMA.

Fig. 3 shows the OP results against the average transmit SNR $\overline{\gamma}$ for various schemes, including FAS-RSMA, TAS-RSMA, FAS-NOMA, and TAS-NOMA. First, Fig. 3(a) reveals the impact of common power allocation factor $\alpha_{\rm c}$ on the OP performance, focusing on the comparison between RSMA and NOMA. Then, in Fig. 3(b), the OP is analyzed for varying the numbers of fluid antenna ports N_k, while maintaining a constant fluid antenna area of $W_k = 1\lambda^2$. Finally, Fig. 3(c) examines the OP for different fluid antenna sizes, keeping the number of ports fixed at $N_k = 9$. In all instances, we can observe that the asymptotic results closely align with the OP curves in the high-SNR regime, confirming the accuracy of our theoretical analysis for both MUs.

In Fig. 3(a), we study the OP performance by varying the power allocation factors[5] over the users. It becomes evident that FAS-based strategies offer a sustained performance improvement over TAS-ones, improving the OP decay through a better diversity order. While for NOMA, the best balance between users in terms of OP is obtained, such performance can also be mimicked by a different power allocation strategy through RSMA. Hence, RSMA brings additional flexibility and robustness over NOMA thanks to the possibility of separately tuning the power allocation for the private and common streams. As the common message power allocation factor $\alpha_{\rm c}$ increases, the OP of the near MU u_2 decreases due to its ability to efficiently decode common and private messages. However, this comes at the expense of the far MU u_1, whose performance degrades as less power is allocated to its private stream. This trade-off highlights a fundamental design consideration in RSMA systems, where tuning $\alpha_{\rm c}$ enables flexible control over user fairness and system throughput.

Let us now focus on the performance improvements of the FAS-RSMA scheme as the fluid antenna parameters change. Fig. 3(b) shows that increasing N_k for a fixed fluid antenna size W_k, improves the OP performance. This enhancement is attributed to the simultaneous gains in channel capacity, diversity, and multiplexing offered by a denser fluid antenna configuration. Furthermore, Fig. 3(c) shows that a larger fluid antenna size W_k, with a fixed N_k, results in a lower OP. This improvement stems from the reduced spatial correlation between antenna ports, as greater physical separation lowers interference and increases spatial diversity. Again, FAS significantly outperforms TAS across all scenarios, owing to its dynamic aperture reconfiguration capability, which enhances spatial diversity and channel adaptability. Although TAS-RSMA benefits from the rate-splitting technique, it is less effective in managing interference. For instance, as observed in Fig. 3(c), at $\overline{\gamma} = 50$dB, the performance gap between FAS-RSMA and TAS-RSMA is remarkable, with FAS-RSMA achieving an OP of about 10^{-6} compared to TAS-RSMA's 10^{-2}. This demonstrates that FAS-RSMA maintains better performance even at lower SNR levels, thanks to the capability of FAS and its ability to respond to environmental changes.

While FAS-RSMA offers significant performance benefits, it is important to acknowledge some potential drawbacks in practical implementations. The integration of FAS with RSMA introduces additional complexity in system design, channel estimation, and signal processing. Managing multiple ports and handling the transmission of both common and private messages across users requires more improved system architectures compared to traditional single-port systems. Besides, channel estimation protocols need to be adapted to facilitate channel estimation and reconstruction at the receiver ends. Despite these challenges, the benefits of FAS-RSMA such as enhanced performances and flexible interference management, make it a promising approach for future wireless systems.

Beyond implementation concerns, the integration of FAS with RSMA presents a number of research challenges. For the specific case under consideration, i.e., RSMA implemented with single-antenna BS and FAS-equipped users, the key challenges are associated with message encoding and power allocation at the BS side (RSMA-related) and channel reconstruction/port selection at the receiver sides (FAS-related). In this scenario, FAS is leveraged at each user end to improve its own OP when operating at a certain rate with some power allocation. While these two processes (RSMA design and FAS port selection) could be jointly designed for optimal operation, that would require an exceeding complexity that may affect the practicality of the scheme. This work serves as a first stepping stone into the integration of RSMA and FAS, and the next step forward should embrace RSMA-FAS in multi-antenna deployments at the BS. The combined features of precoding at the BS and port selection at the FAS have the ability to offer additional improvements in terms of interference mitigation, and definitely deserve further consideration as a powerful synergy in the future evolution of wireless system.

V. Conclusion

In this letter, we explored the performance of FAS-aided RSMA in downlink multiuser communications. First of all, we derived an analytical expression for the OP based on the joint CDF of the multivariate t-distribution and examined the system's asymptotic behavior in high-SNR conditions. Our

[4]Note that while we consider a two-user system ($K = 2$) for simplicity in the simulations, the theoretical derivations are valid for a general K-user system, ensuring broader applicability of the results.

[5]For this $K = 2$ setup, NOMA can be seen as a special case of RSMA by setting $w_1 = w_{\rm c}$ and $w_2 = w_{\rm p,2}$ in Fig. 2, with $\alpha_{\rm p,1} = 0$ [11].

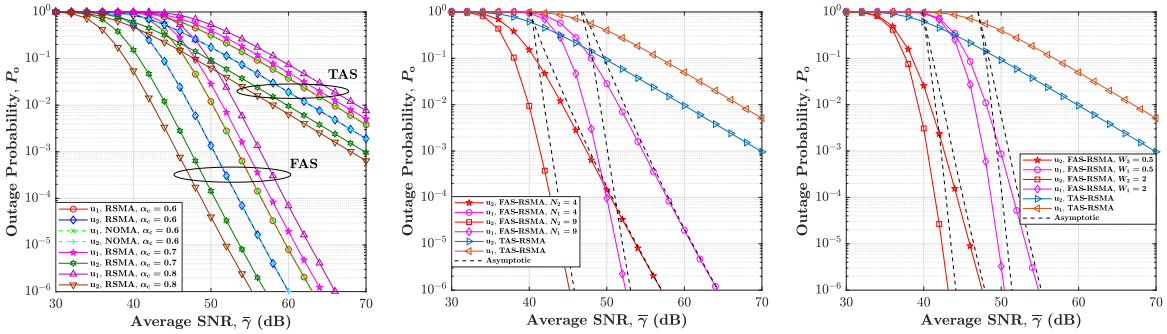

(a) (b) (c)

Fig. 3. OP vs. the average transmit SNR $\bar{\gamma}$: (a) for different common power allocation factor α_c, (b) for different numbers of fluid antenna ports N_k with a fixed $W_k = 1\lambda^2$, and (c) for different values of fluid antenna size with a fixed $N_k = 9$.

findings demonstrated that FAS combined with RSMA delivers notable improvements over TAS and NOMA. These results highlight the effectiveness of integrating fluid antenna technology with advanced communication strategies for significantly enhancing system reliability and performance.

Appendix A
Proof of Proposition 1

By applying Sklar's theorem from (14) to the CDF definition in (13), $F_{g_{\text{fas},k}}(g)$ can be rewritten as

$$F_{g_{\text{fas},k}}(g) = C\left(F_{g_k^1}(g), \ldots, F_{g_k^{N_k}}(g); \Theta_k\right), \tag{21}$$

where $C(\cdot)$ can be any arbitrary copula and $F_{g_k^{n_k}}(g)$ is the marginal CDF of the channel gain, which follows exponential distribution due to Rayleigh fading channels, i.e., we have $F_{g_k^{n_k}}(g) = 1 - \mathrm{e}^{-g/\overline{g}}$, where $\overline{g} = \mathbb{E}[g]$ is the mean of the channel gain. Following the insights provided in [16], revealing the fact that elliptical copula can accurately approximate Jakes' model in FAS, we exploit the t-student copula, which captures positive/negative and linear/non-linear correlations as well as heavy tail dependencies and it is defined as [17]

$$C(u_1, \ldots, u_d) = T_{\nu,\mathbf{\Sigma}}\left(t_\nu^{-1}(u_1), \ldots, t_\nu^{-1}(u_d); \nu, \Theta\right), \tag{22}$$

in which $t_\nu^{-1}(\cdot)$ denotes the quantile function of the univariate t-distribution with ν degrees of freedom, $T_{\nu,\mathbf{\Sigma}}(\cdot)$ is the CDF of the multivariate t-distribution with correlation matrix $\mathbf{\Sigma}$ and ν degrees of freedom, and $\Theta \in [-1, 1]$ represents the dependence parameter of t-student copula, which measures the correlation between two arbitrary RVs. It should be noted that the t-student copula is a more general instance of the elliptical copula, which approaches the Gaussian copula as the degrees of freedom ν becomes large, i.e., $\nu \to \infty$. Moreover, it was shown in [16] that the dependence parameter of the elliptical copula such as the Gaussian copula is almost equal to the correlation coefficient derived by Jakes' model, i.e., $\Theta_k \approx \varrho_{n_k,\tilde{n}_k}$. Hence, upon applying (22) to (21), we have

$$F_{g_{\text{fas},k}}(g) = T_{\nu_k,\mathbf{R}_k}\left(t^{-1}\left(F_{g_k^1}(g)\right), \ldots, t^{-1}\left(F_{g_k^{N_k}}(g)\right); \nu_k, \Theta_k\right). \tag{23}$$

Finally, by inserting $F_{g_k^{n_k}}(g)$ into (23), (16) is derived. Also, by using the definition of the copula PDF and applying the chain rule to (22) [15], (17) is therefore obtained.

References

[1] X. You *et al.*, "Toward 6G TKμ extreme connectivity: Architecture, key technologies and experiments," *IEEE Wirel. Commun.*, vol. 30, no. 3, pp. 86–95, Jun. 2023.

[2] K.-K. Wong, K.-F. Tong, Y. Zhang, and Z. Zheng, "Fluid antenna system for 6G: When Bruce Lee inspires wireless communications," *Elect. Lett.*, vol. 56, no. 24, pp. 1288–1290, Nov. 2020.

[3] W. K. New *et al.*, "A tutorial on fluid antenna system for 6G networks: Encompassing communication theory, optimization methods and hardware designs," *IEEE Commun. Surv. & Tut.*, doi:10.1109/COMST.2024.3498855, 2024.

[4] K.-K. Wong, A. Shojaeifard, K.-F. Tong, and Y. Zhang, "Fluid antenna systems," *IEEE Trans. Wirel. Commun.*, vol. 20, no. 3, pp. 1950–1962, Mar. 2021.

[5] W. K. New, K.-K. Wong, H. Xu, K.-F. Tong, and C.-B. Chae, "An information-theoretic characterization of MIMO-FAS: Optimization, diversity-multiplexing tradeoff and q-outage capacity," *IEEE Trans. Wirel. Commun.*, vol. 23, no. 6, pp. 5541–5556, Jun. 2024.

[6] Y. Ye *et al.*, "Fluid antenna-assisted MIMO transmission exploiting statistical CSI," *IEEE Commun. Lett.*, vol. 28, no. 1, pp. 223–227, Jan. 2024.

[7] F. R. Ghadi *et al.*, "On performance of RIS-aided fluid antenna systems," *IEEE Wirel. Commun. Lett.*, vol. 13, no. 8, pp. 2175–2179, Aug. 2024.

[8] C. Wang *et al.*, "Fluid antenna system liberating multiuser MIMO for ISAC via deep reinforcement learning," *IEEE Trans. Wirel. Commun.*, vol. 23, no. 9, pp. 10879–10894, Sept. 2024.

[9] J. Zhang *et al.*, "A novel pixel-based reconfigurable antenna applied in fluid antenna systems with high switching speed," *IEEE Open J. Antennas & Propag.*, vol. 6, no. 1, pp. 212–228, Feb. 2025.

[10] Y. Mao, B. Clerckx, and V. O. Li, "Rate-splitting multiple access for downlink communication systems: Bridging, generalizing, and outperforming SDMA and NOMA," *EURASIP J. Wirel. Commun. Netw.*, vol. 2018, pp. 1–54, May 2018.

[11] B. Clerckx, Y. Mao, R. Schober, and H. V. Poor, "Rate-splitting unifying SDMA, OMA, NOMA, and multicasting in MISO broadcast channel: A simple two-user rate analysis," *IEEE Wirel. Commun. Lett.*, vol. 9, no. 3, pp. 349–353, Mar. 2020.

[12] W. K. New *et al.*, "Fluid antenna system enhancing orthogonal and non-orthogonal multiple access," *IEEE Commun. Lett.*, vol. 28, no. 1, pp. 218–222, Jan. 2024.

[13] W. K. New *et al.*, "Channel estimation and reconstruction in fluid antenna system: Oversampling is essential," *IEEE Trans. Wirel. Commun.*, vol. 24, no. 1, pp. 309–322, Jan. 2025.

[14] Z. Chai *et al.*, "Port selection for fluid antenna systems," *IEEE Commun. Lett.*, vol. 26, no. 5, pp. 1180–1184, 2022.

[15] F. R. Ghadi and G. A. Hodtani, "Copula-based analysis of physical layer security performances over correlated Rayleigh fading channels," *IEEE Trans. Inf. Forensics Security*, vol. 16, pp. 431–440, 2020.

[16] F. R. Ghadi *et al.*, "A Gaussian copula approach to the performance analysis of fluid antenna systems," *IEEE Trans. Wirel. Commun.*, vol. 23, no. 11, pp. 17573–17585, Nov. 2024.

[17] A. Sundaresan, P. K. Varshney, and N. S. Rao, "Copula-based fusion of correlated decisions," *IEEE Trans. Aerosp. Electron. Syst.*, vol. 47, no. 1, pp. 454–471, Jan. 2011.